# Single nanowire measurements of room temperature ferromagnetism in FeSi nanowires and the effects of Mn-doping.

Ángel R. Ruiz<sup>1</sup>, José Hernández-Pérez<sup>1</sup>, Luis F. Fonseca<sup>1</sup>, Miguel José-Yacamán<sup>2</sup>, Eduardo Ortega<sup>2</sup> and Arturo Ponce<sup>2</sup>

E-mail: luis.fonseca@upr.edu

Received xxxxxx Accepted for publication xxxxxx Published xxxxxx

### Abstract

Semiconductors with magnetic response at room temperature are sought for spintronics in solid-state devices. Among possible materials for this applications, the magnetic response of FeSi and doped FeSi have produced contradictory results at the nanoscale and more precise measurements and deeper studies are needed to clarify its potential capabilities. For that reason, in this work, single nanowire measurements of ferromagnetic semiconducting FeSi and Mn-doped Fesi nanostructures have been performed using magnetic force microscopy and electron holography. Results obtained confirm the presence of magnetic domains at room temperature with a magnetic moment per Fe atom of  $0.69\mu_B$ . Spin polarized density functional calculations confirm a net magnetic moment between  $0.4\mu_B - 1.3\mu_B$  in Fe surface atoms with an estimated Curie temperature of 417K by means of the molecular field approximation. The nanowires present a crystalline B20 cubic structure as confirmed by X-Ray diffraction and high-resolution electron microscopy. Their electrical transport measurements confirm p-type nature and thermal activation. A remanent magnetization of 1.5 X  $10^{-05}$  emu and 0.5 X  $10^{-05}$  emu was measured at room temperature for FeSi and Mn-doped FeSi respectively, with spin freezing behavior around 30 K for the Mn-doped nanowires.

Keywords: nanowires, semiconductor, ferromagnetism, FeSi,

### 1. Introduction

The access of room temperature magnetic semiconducting nanomaterials compatible with novel electronic circuits is of great importance for the development of spintronics devices.[1] To this end, some magnetic semiconductors like Mn-doped (ZnO, GaN) and transition metal doped titanium dioxide dilute semiconductors have been synthesized, showing ferromagnetic properties at room temperature at low doping concentrations [6, 19, 25, 30]. However, work must be done to implement non-Si dilute semiconductor in Si

based devices [8, 33]. For steering the efforts on the already developed Si technology many works have been performed on transition metal silicides, showing low temperature ferromagnetism in some of these silicides like MnSi and Fe<sub>1</sub>.  $_x$ Co $_x$ Si which present helimagnetic states at 3K and 37K, respectively [4, 14]. Nevertheless FeSi, one of the few semiconducting material in the family of the transition metal silicides, is characterized by the absence of such states in bulk samples.[22]

<sup>&</sup>lt;sup>1</sup> Department of Physics, University of Puerto Rico-Río Piedras Campus, San Juan, Puerto Rico

<sup>&</sup>lt;sup>2</sup> Department of Physics and Astronomy, University of Texas at San Antonio, San Antonio, United States

The transition of some of these silicides to nanowires have shown promising magnetic response. CoSi nanowires have reported to be ferromagnetic above temperature[27] compared to their diamagnetic bulk counterpart. Moreover, some studies on FeSi and Mn-doped  $Fe_{1-x}Mn_xSi$ (FeMnSi) nanowires have presented ferromagnetism at room temperature.[12, 13] However, due to its low remanent magnetization at room temperature and its magnetic properties being measured in as-grown samples, the magnetic properties of FeSi are in controversy, being reported as a paramagnetic material by some authors.[26] To the best of our knowledge, magnetic studies on single FeSi and Mn-doped FeSi nanowires have not been reported. In this work we present the synthesis and measured magnetic response of these semiconductor materials with an estimation of its Curie temperature using spin polarized density functional theory (DFT) in conjunction with the mean field approximation (MFA) on single nanowires. Nanowires have been chosen as the subject of study due to their inherent shape anisotropy, small diameters, large and smooth surface areas. They can exhibit tunable and different magnetic properties than their thin films counterparts,[32] making them promising new building blocks for the development of novel devices and ideal for electrical integration. [8]

### 2. Experimental

FeSi and FeMnSi nanowires were synthesized by Chemical Vapor Deposition (CVD). The synthesis approach was based on the Arkel method which separates the metal through vapor transport. [35] The metal halide precursor (FeCl<sub>3</sub>) was placed inside a quartz tube at the upstream zone of a conventional two-zone horizontal hot-wall furnace. Once on its gaseous state, the precursors were transported with a 300 sccm N<sub>2</sub> flux towards a Si (1 1 1) substrate, previously washed and etched using a 10% hydrofluoric acid solution, at the downstream zone. The physical conditions for the synthesis of FeSi nanowires were: a temperature of 900 C and a pressure of 1 atm at the downstream zone, where the gaseous precursor reacted with the Si substrate to form the free-standing nanowires. The change of phase of the anhydrous FeCl<sub>3</sub> precursor started around 350 C at the upstream zone. Both zones shared similar pressure and their temperatures where independently controlled. Anhydrous MnCl<sub>2</sub> was additionally placed at the upstream zone for the synthesis of FeMnSi nanowires. Similarly, the upstream temperature was independently controlled for the sublimation of the precursors around 350 C, in which they were transported with a 300 sccm N<sub>2</sub> flux to the downstream zone, reacting with the previously washed and etched Si substrate to form the FeMnSi nanowires.

The morphology and structural characterization of the synthesized nanowires was performed in a JEOL 2010F microscope operated at 200 kV and with a Rigaku X-Ray

diffractometer with Cu-K alpha radiation. The doping of the samples was studied with energy-dispersive X-ray spectrometry (EDS).

# 3. Results and Discussion

The CVD method produces a high yield of homogenous nanowires as observed on the low magnification SEM images on Fig 1a and 2a. The as grown FeMnSi and FeSi nanowires present diameters from 25nm and have a native SiO<sub>x</sub> layer covering the surface. (Fig 1b, Fig2b). SAED and HRTEM measurements suggest a highly crystalline nature for both materials. FeSi nanowires have the plane (1 1 0) parallel to the growth direction as seen on Fig 1b. FeMnSi nanowires are found to grow in the (1, -1, 0) direction with the plane (111) parallel to the nanowire's growth direction (Fig 2b). The presence of Mn was confirmed by EDS, with doping levels around 1% (Fig 2d and Fig S1 of the Supplementary Information). The XRD patterns (Fig 1c and Fig 2c) confirm the crystalline nature of both materials (FeSi and FeMnSi), showing the B20 cubic crystal pattern of FeSi, with a lattice parameter of 0.448 nm. By having the same equilibrium structure as its other analogue MnSi, the replacement of Fe at the transition metal site is easily accomplished forming a diluted semiconductor while holding the same crystal structure. [5, 28]

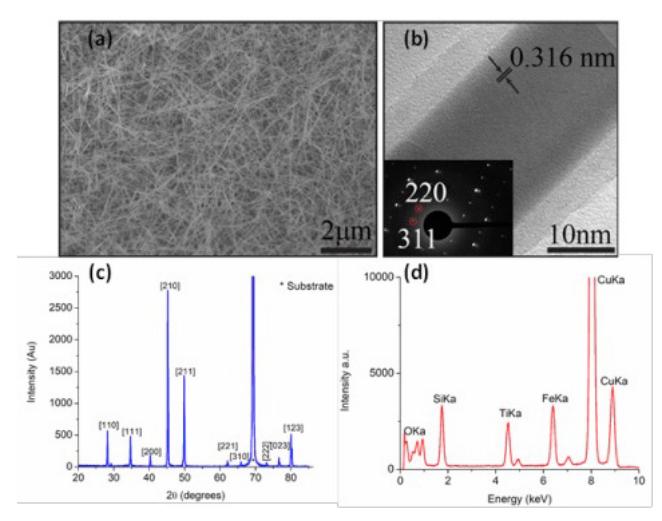


Fig 1 – (a) SEM mage of as grown FeSi nanowires. b) HRTEM and SAED (inset). The plane (1 1 0) is parallel to the nanowires growth direction. c) XRD of FeSi nanowires showing a B20 cubic crystal structure. d) EDS measurements of FeSi. Results indicate a 1:1 ratio of Fe and Si.

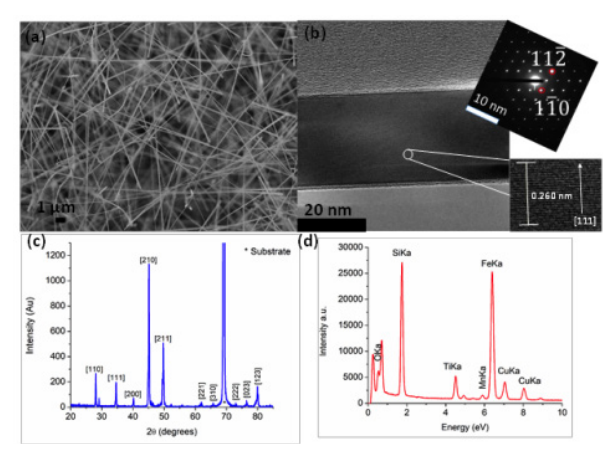


Fig 2 – (a) SEM image of as grown FeMnSi nanowires. b) HRTEM and SAED (inset). The (1 1 1) plane is parallel to the nanowires growth direction. c) XRD of FeMnSi nanowires showing a B20 cubic crystal structure. d) EDS measurements of FeMnSi. Results indicate a 1.7% of Mn doping.

The absence of metal catalysts at the tip of the synthesized nanowires supports the self-assembled growth of nanowires by a vapor-solid mechanism. When the thermodynamic condition were reached at the downstream zone, the gaseous precursors could react in the two following ways with the Si substrate to form the FeMnSi nanowires: [12]

$$\begin{split} &2(Mn,Fe)Cl_{(2,3)(g)} + 3Si_s \to 2Fe_{1\text{-}x}Mn_xSi_{(s)} + SiCl_{4(g)} \\ &SiCl_{4(g)} + (Mn,Fe)Cl_{(2,3)g} \to Fe_{1\text{-}x}Mn_xSi_{(s)} + 3Cl_{2(g)} \end{split}$$

Direct measurements of standard enthalpies of formation of the silicides show that the exothermic reaction favors the formation of FeSi over its counterpart MnSi because of its lower enthalpy, [20] with the additional fact that the enthalpy of formation of the MnCl<sub>2</sub> is lower than FeCl<sub>3</sub>. These factors together contribute to the formation of FeMnSi nanowires, more energetically favorable than MnSi.

Information about the electrical transport properties of the nanowires was retrieved by means of specialized microbridge thermometry devices.[24] Fig 3 shows FeSi and FeMnSi nanowires connected over Pt microelectrodes to perform four-points conductivity measurements. The devices include two platinum resistor thermometers at the ends of the nanowire that allow to create a thermal gradient through the nanowire and to measure the thermoelectrical voltage. In Fig 3d the conductivity of FeSi appears thermally activated, this result is consistent with the fact that bulk FeSi is widely known to be a semiconductor with a band gap of 0.13 eV. [37] The electrical transport properties of the FeSi nanowire were also calculated based on the Boltzmann transport equation under the rigid band and constant relaxation time approximations as implemented in the BoltzTraP numerical package. To do so, first density functional theory (DFT) calculations were performed using the Vienna Ab initio Simulation Package (VASP).[16] The many-body LDA

approximation was implemented with the projector augmented wave (PAW)[2]. The energy cut-off for the plane wave expansion was 300 eV. The Brillouin zones were sampled in a gamma-centered grid with a k-point mesh of 15 x 15 x 15. To obtain an accurate DOS, the k-point mesh of the non-self-consistent calculation was increased to 37×37×37. Atomic positions and unit cell vectors were relaxed until all the forces and components of the stress tensor are below 0.001 eV Å<sup>-1</sup>. Bulk parameters were used for the calculations because the diameter of the simulated nanowire is greater than 20nm. Starting from the experimental B20 cubic crystal with lattice parameter a =4.375 Å, the calculated indirect bandgap  $(E_{\sigma})$  was 0.146 eV, which is slightly different than the experimental bandgap.[23, 29] When carrying out the transport calculations the energy results were corrected for this by manually adjusting the gap to the experimental value. It is worth to emphasize that this correction does not alter the value of dispersive quantities (group velocity, effective masses) used in the transport calculations.[38] For the transport calculations, a correlation between the Seebeck coefficient at different temperatures using the results from Wolfe et al. [34, 36] and the conductivity/relaxation time from BotlzTrap was made for the following temperatures: 120K-370K with a temperature grid of 50K. Using the measured conductivity data obtained at 320K (figure 3d), an estimated relaxation time was obtained. The correlated electrical conductivity given by BoltzTraP is presented in figure 3d as red dots. The theoretical results fit the experimental data. Moreover, experimental results for the conductivity of FeSi obtained in reference [21] feature similar values (~2.5 x10<sup>5</sup> S/m) at room temperature for nanowires. The results for bulk single crystals [34] also show conductivity values within the same magnitude range (~2X 10<sup>5</sup>) S/m. The measured Seebeck coefficient of a FeMnSi nanowire at 310K was +23.08µV/K which confirms the p-type nature of the semiconductor in this range of temperatures, as its bulk counterpart.

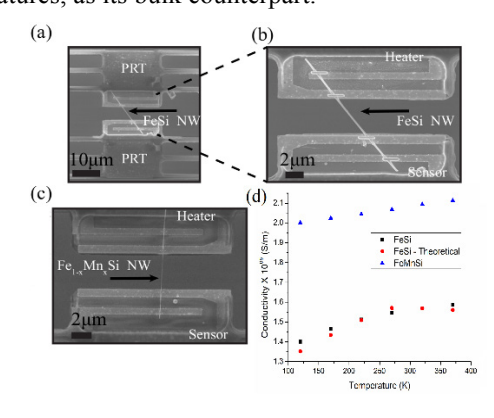


Fig-3 a,b,c) FeSi and FeMnSi nanowires on four point probes measuring microdevices. d) Conductivity vs Temperature for FeSi and FeMnSi nanowires and theoretical fitting (red dots). Results suggest a semiconducting behavior for both nanowires. Mn doping improves the electrical transport in FeSi nanowires.

The presence of a ferromagnetic phase at room temperature on single FeSi and FeMnSi nanowires was confirmed by means of room temperature magnetic force microscopy (MFM) using a Veeco multi-mode scanning probe microscope with a CoCr coated tip. Results show that the nanowires behave as two-domain magnetic structure. The MFM images were generated by recording the phase of the cantilever oscillation in lift-mode with the cantilever out of contact. The evident bright and dark contrast in Fig 4b are the results of the magnetization perpendicular to the nanowires growth axis, as can been seen in a change in the cantilever frequency in Fig 4c, d. This change in frequency (green line) is proportional to the force acting on the tip[31] as seen in Fig 4d. Assuming that the tip consists of a point dipole with effective magnetic moment m, the force acting on the tip can be described as  $F_{mag} = \nabla(m \cdot h)$ , where h is the stray field from the sample.[9] Fig 4a presents the topographic image of two nanowires with about 40 nm in diameter as seen on Fig 4c (red line). The presence of two domains presented on Fig 4b can be explained by means of the anisotropy characteristic length, understood as the required length for twisting a unit angle in the exchange coupled chain of magnetic moments. This have been seen in micromagnetic modeling of Co nanowires were a uniform magnetic configuration is the lower energy state for thin wires (<40 nm), while thicker wires produce magnetization patterns with vortices. [17] Fig 4e depicts the magnetic structure for z-vortices in which the magnetization remains constant through the nanowires growth axis (z axis in Fig 4e). Y-vortices (in which the magnetization remains constant in the nanowire's transverse direction) tend to be energetically more common as the diameter increases. At about 110nm both phases are equally favored. Results presented on the MFM measurements confirm magnetization perpendicular to the z-axis as seen in the x-y cross section of the FeSi and FeMnSi nanowires, an expected result for such diameter range according to calculations. [17] Similarly, Figs 5a and 5b present the topographic and magnetic mappings of a 85 nm FeMnSi nanowire. The nanowires posses z-vortices magnetic configurations as its counterpart FeSi. Note the higher frequency change in the FeSi nanowires. Tough it has been reported that FeMnSi nanowires holds higher magnetization when measured in the as-grown substrate,[12] the presented FeSi nanowire is two times thinner and the magnetization of the nanowires is expected to increase when reducing its diameter due to the increasing ratio of dandling bonds and magnetocrystalline anisotropy considered responsibles of the nanowires magnetism. [11, 15] More AFM/MFM mappings of other FeSi and FeMnSi nanowires are included in Fig. S2 and Fig. S3 of the Supplementary Information, respectively.

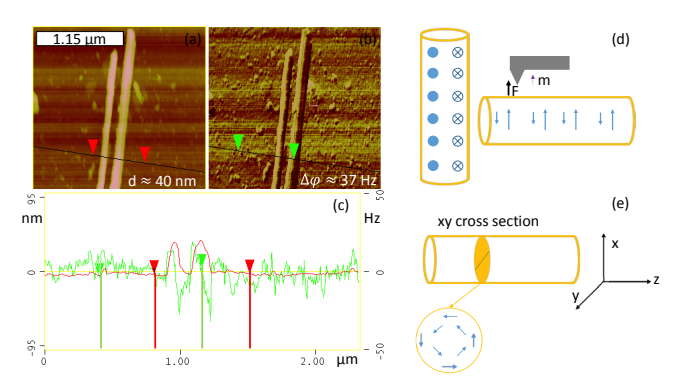


Fig 4: (a)Topographic AFM image of two FeSi nanowires. Bright colors correspond to an increase in altitude. (b) MFM image of two FeSi nanowires. Bright colors correspond to an increase while dark colors correspond to a decrease of the natural cantilever frequency. (c) Numerical profile of the scanned area, featuring the nanowires diameter (red) and samples stray field (green) which is proportional to the cantilever change in frequency. (d) Schematic representation of the magnetic force acting on the cantilever. (e) Representation of the z-vortices seen on the nanowires. Note how the magnetization doesn't vary on the z direction as seen on the MFM images.

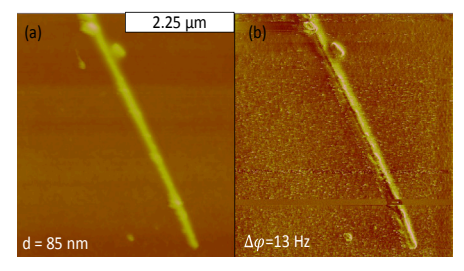


Fig 5: a) Topographic AFM image of a FeMnSi nanowire. Results show a diameter of 85nm for the nanowire. (b) MFM image. A change of frequency of 13 Hz was obtained. The nanowires show similar magnetic configuration as FeSi, remaining constant through the nanowire's growth direction.

Quantitative magnetometry analysis of the remanent state over a single FeMnSi nanowire in the TEM was performed using Off-axis electron holography (EH). Using an electron biprism (DC biased tungsten wire under the plane of the sample) an electron hologram was acquired as shown in Fig. 6a. The hologram is correlated with an image reference (one without the nanowire) to retrieve the phase information of the electron wave after its magnetic interaction with the sample. The phase image in Fig 6b represents only the integrated in-plane magnetic induction and was obtained subtracting two different electron holograms with opposite magnetization directions (Fig S4 - Supplementary information) in a way to get rid of electrostatic/crystalline potentials. The color change in this Fig represents a phase jump over the two regions on the vicinity of the FeMnSi nanowire. From the phase shift  $(\Delta \varphi)$  over length  $(\Delta x)$  (Fig 6c), the magnetic flux density can be calculated from the following relation  $B = (\overline{h}/e \cdot t) \cdot \frac{\delta \varphi}{dx}$ , where 't' is the NW thickness, and e and  $\overline{h}$  are constants.[3] From the phase shift of approximately 6.5 radians the magnetic induction was quantitatively evaluated as B = 0.69 T.

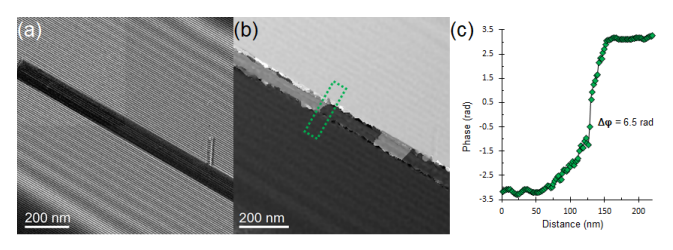


Fig 6 - (a) Electron hologram of a single FeMnSi NW, (b) Magnetic contribution obtained after subtracting two phase images with opposite remnant magnetization, (d) phase profile from (b) showing the phase jump between the two regions separated by the

The magnetic moment per iron atom can be estimated considering that Mn only represents a ~1% of the total magnetization. In Bohr magnetons it is given as  $\mu = 1.07828 \times 10^{20} \frac{\mu_B}{emu} \frac{M_{mole}}{N_A} \frac{B(\frac{emu}{cm^3})}{\rho} \gamma$ , where  $\Upsilon$  is the fraction of iron atoms, B is the magnetic field in emu/cm³,  $\rho$  is the density of FeSi in g/cm³ and  $M_{mole}$  the molecular weight of FeSi. The obtained magnetic moment per Fe atom in the FeMnSi nanowire was  $0.65~\mu_B$ .

The magnetic properties of the as-grown FeMnSi and FeSi nanowires were also measured in vacuum using a Physical Property Measurement System (PPMS) magnetometer. Measured samples were as-grown CVD samples deposited on 3.5mm x 3.5mm Si substrate (FeSi) and 4mm x 4mm Si substrate (FeMnSi), respectively. High temperature measurements (up to 800K) were done on FeMnSi samples. Results in Fig 7a show the contribution of the nanowire's magnetic moment at different temperatures as a function of the external magnetic field. The magnetic contribution of the Si substrate is 10<sup>-06</sup> emu[27], thus can be ignored. Both materials exhibit ferromagnetism at room temperature but at 800K FeMnSi shows almost no remanent magnetization. Fig 7b presents field cooling (FC) and zero-field cooling (ZFC) measurements. Peaks in the curves can be seen at low temperatures (around 10K) for both materials that could be related to spin freeze like behavior while FeMnSi seems to enter another spin disorder phase around 150k. However, the cooling rate of the sample was 12 sec/K and poor thermalization effects cannot be discarded at low temperature due to the nanostructured organization of the sample. AC susceptibility measurments were not available to complement these observations. Nevertheless, because the HRTEM, XRD and EDS measurements indicate highly crystalline materials, the origin of high temperature ferromagnetism in FeSi and FeMnSi nanowires is associated to the uncoordinated transition metal atoms and interaction of charge carriers with dangling bonds in the surface region of the nanowire (where disorder is favored) and not due to strains or structural defects within the nanowire.

Low temperature FC and ZFC cycles were done after the hysteresis measurements, thus a discontinuity is observed between ZFC high temperature cycle and the low temperature one, while it is not observed in the FC curve because the high temperature hysteresis curve was measured when reaching 800K.

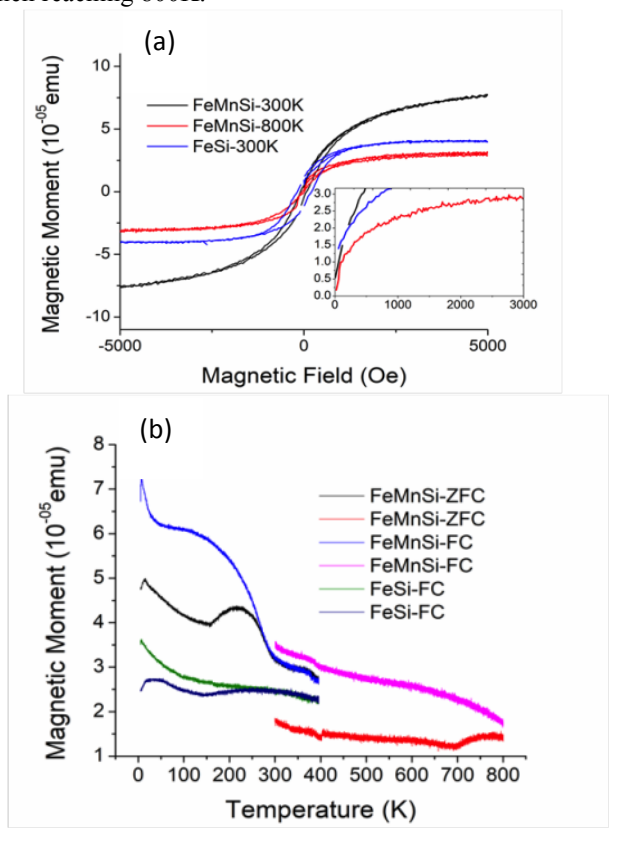


Fig 7-a) M-H measurements of FeSi and FeMnSi nanowires. Results show ferromagnetism at room temperature for both materials. b) FC and ZFC measurements of FeSi and FeMnSi nanowires. Spin freeze behavior is observed at low temperatures around 30 K.

For the calculation of the ferromagnetic phases of these semiconductor nanowires, first principle simulations were performed using VASP in a (1 1 1) slab and a supercell of 24 Fe and 24 Si atoms was built (Fig 8b). The many-body LDA approximation was implemented with the PAW scheme [2]. The energy cut-off for the plane wave expansion was 300 eV. The Brillouin zones were sampled in a gammacentered grid with a k-point mesh of 8 x 8 x 1.

Results in Fig 8a present the magnetic moment of Fe and Si atoms as a function of their position in fractional coordinates suggesting that the origin of magnetism in iron silicide nanowires has its major contribution from the nanowire's surface atoms as already suggested [7]. Nevertheless, to confirm the existence of a ferromagnetic phase in FeSi the energy difference between a ferromagnetic and antiferromagnetic coupling was calculated. We chose an inplane alignment for the anti-ferromagnetic calculations. Results gave a total energy difference of 0.162eV. By means of the direct exchange interaction and mean field

approximation (MFA), the Curie temperature for FeSi can be expressed as

$$T_c = \frac{4\left(1 + \frac{1}{S_z}\right)(E_{\downarrow} - E_{\uparrow})}{27 * 8.617 \times 10^{-05} eV \cdot K^{-01}}$$
$$= \frac{E_{\downarrow} - E_{\uparrow}}{1.163295 \times 10^{-03} eV T^{-1}}$$

Therefore, the calculated Curie temperature for the (1 1 1) slab on FeSi is 417 K.

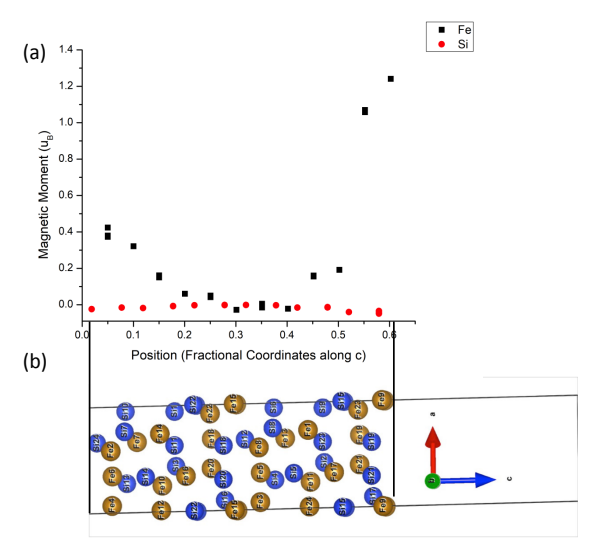


Fig 8 - a) magnetic moment of Si and Fe atoms relative to their position. (b) Super cell used for the FeSi DFT calculations. Boundaries are the labeled 24 Si atom and the 9 Fe atom with 0 and 0.6 positions, respectively.

The effects of Mn doping on the silicide can be estimated by replacing a Fe atom by a Mn one in the supercell giving rise to a 2% doping. Since a FeSi nanowire is a magnetic material and Mn concentration is low, the contribution of the Fe-Fe direct magnetic exchange interaction cannot be discarded in FeMnSi, therefore we estimated the Curie temperature of the FeMnSi (1 1 1 ) slab using the direct exchange Heisenberg Hamiltonian and MFA. Results render higher Curie temperatures and the total magnetizations are more noticeable when the Mn atoms are placed near the interfaces, as shown in Fig 9. All these calculations support that the origin of magnetism in these nanowires is a surface effect and the reason of the absence of helimagnetic phase in both, bulk FeSi and FeMnSi.[18] A high Curie temperature of~ 800 K was obtained for FeMnSi however, it is well known that MFA calculations overestimate the Curie temperature. [10]

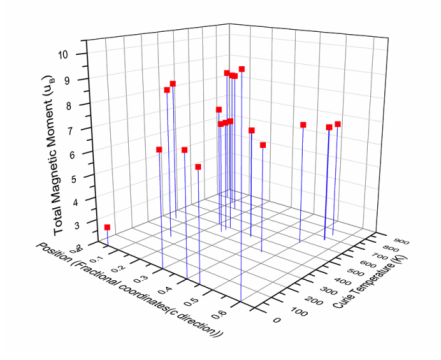


Fig 9 – DFT results. The position represents the places were the Fe atom was replaced by Mn. The Curie temperature was calculated by taking the energy differences between the ferromagnetic and anti-ferromagnetic configuration. 0 values in Curie temperature correspond to a non-ferromagnetic phase.

# 3. Conclusion

In conclusion, experimental studies and computational results about the magnetic and electrical properties of FeSi and Fe<sub>1-x</sub>Mn<sub>x</sub>Si nanowires are presented that support the existence of a room temperature ferromagnetic phase on semiconducting FeSi and FeMnSi nanowires grown by CVD. XRD, HRTEM, SAED, EDS and electrical transport characterization were all consistent with the successful synthesis of highly crystalline quality ε-FeSi phase. Electron holography and MFM mappings confirm the presence of room temperature magnetism when testing single nanowires and discard the presence of small Fe<sub>3</sub>Si precipitates as the source of their magnetic response. DFT calculations demonstrate that the transition metal atoms near the interface are the major players for the existence of a ferromagnetic phase in both materials and give Curie temperatures which vary with the Mn position in the case of FeMnSi. These results support the already proposed theory of dandling bonds in the silicide as responsible of the ferromagnetism at room temperature in these nanowires.

## Acknowledgements

Work partially supported by NSF Grant HRF-1736093. The DFT calculations were performed using the facilities of Holland Computer, University of Nebraska – Lincoln. A. R. R. Acknowledges support from Puerto Rico NASA Space Consortium #NNX15A11IH, and NSF PR-LSAMP Grant HRD1139888, and thanks Dr. Renat Sabirianov, University of Nebraska - Omaha for facilitating the access to the facilities and helpful discussions. The transmission electron microscopy work in the Kleberg Advanced Microscopy Center was supported by the National Institute on Minority Health and Health Disparities (G12MD007591) of the National Institutes of Health (NIH).

## References

- [1] Awschalom D D and Flatté M E 2007 Challenges for semiconductor spintronics *Nature Physics* **3** 153
- [2] Blöchl P E 1994 Projector augmented-wave method *Physical Review B* **50** 17953-79
- [3] Cantu-Valle J, Betancourt I, Sanchez J, Ruiz-Zepeda F, Maqableh M, Mendoza-Santoyo F, Stadler B and Ponce A 2015 Mapping the magnetic and crystal structure in cobalt nanowires vol 118
- [4] Chattopadhyay M K, Roy S B, Chaudhary S, Jeet Singh K and Nigam A K 2002 Magnetic response of \${\mathrm{Fe}}\_{1\ensuremath{-}}x} {\mathrm{Co}}\_{x}\mathrm{Si}\$ alloys: A detailed study of magnetization and magnetoresistance *Physical Review B* **66** 174421
- [5] DiTusa J F 2016 *Handbook of Spintronics*, ed Y Xu, *et al.* (Dordrecht: Springer Netherlands) pp 523-61
- [6] Edmonds K W, Farley N R S, Johal T K, van der Laan G, Campion R P, Gallagher B L and Foxon C T 2005 Ferromagnetic moment and antiferromagnetic coupling in (Ga,Mn)As thin films *Physical Review B* 71 064418
- [7] Guo G Y 2001 Surface electronic and magnetic properties of semiconductor FeSi *Physica E: Low-dimensional Systems and Nanostructures* **10** 383-6
- [8] Hayden O, Agarwal R and Lu W 2008 Semiconductor nanowire devices *Nano Today* **3** 12-22
- [9] Henry Y, Ounadjela K, Piraux L, Dubois S, George J M and Duvail J L 2001 Magnetic anisotropy and domain patterns in electrodeposited cobalt nanowires *The European Physical Journal B Condensed Matter and Complex Systems* **20** 35-54
- [10] Hortamani M, Sandratskii L, Kratzer P, Mertig I and Scheffler M 2008 Exchange interactions and critical temperature of bulk and thin films of MnSi: A density functional theory study *Physical Review B* **78** 104402
- [11] Huang, Li L, Luo X, Zhu and Li 2008 Orientation-Controlled Synthesis and Ferromagnetism of Single Crystalline Co Nanowire Arrays *The Journal of Physical Chemistry C* 112 1468-72
- [12] Hung M-H, Wang C-Y, Tang J, Lin C-C, Hou T-C, Jiang X, Wang K L and Chen L-J 2012 Free-Standing and Single-Crystalline Fe1–xMnxSi Nanowires with Room-Temperature Ferromagnetism and Excellent Magnetic Response ACS Nano 6 4884-91
- [13] Hung S-W, Wang T T-J, Chu L-W and Chen L-J 2011 Orientation-Dependent Room-Temperature Ferromagnetism of FeSi Nanowires and Applications in Nonvolatile Memory Devices *The Journal of Physical Chemistry C* 115 15592-7

- [14] Ishikawa Y, Tajima K, Bloch D and Roth M 1976 Helical spin structure in manganese silicide MnSi Solid State Communications 19 525-8
- [15] Kim T, Naser B, Chamberlin R V, Schilfgaarde M V, Bennett P A and Bird J P 2007 Large hysteretic magnetoresistance of silicide nanostructures *Physical Review B* **76** 184404
- [16] Kresse G and Furthmüller J 1996 Efficiency of abinitio total energy calculations for metals and semiconductors using a plane-wave basis set *Computational Materials Science* **6** 15-50
- [17] Lebecki K M and Donahue M J 2010 Comment on "Frustrated magnetization in Co nanowires: Competition between crystal anisotropy and demagnetization energy" *Physical Review B* **82** 096401
- [18] Manyala N, Sidis Y, DiTusa J F, Aeppli G, Young D P and Fisk Z 2004 Large anomalous Hall effect in a silicon-based magnetic semiconductor *Nature Materials* **3** 255
- [19] Matsumoto Y, Murakami M, Shono T, Hasegawa T, Fukumura T, Kawasaki M, Ahmet P, Chikyow T, Koshihara S-y and Koinuma H 2001 Room-Temperature Ferromagnetism in Transparent Transition Metal-Doped Titanium Dioxide Science 291 854
- [20] Meschel S and J. Kleppa O 1994 The Standard Enthalpies of Formation of Some 3d Transition Metal Aluminides by High-Temperature Direct Synthesis Calorimetry
- [21] Ouyang L, Thrall E S, Deshmukh M M and Park H 2006 Vapor-Phase Synthesis and Characterization of ε-FeSi Nanowires *Advanced Materials* **18** 1437-40
- [22] Pearton S 2004 Silicon-based spintronics *Nature Materials* **3** 203
- [23] Perdew J P, Yang W, Burke K, Yang Z, Gross E K U, Scheffler M, Scuseria G E, Henderson T M, Zhang I Y, Ruzsinszky A, Peng H, Sun J, Trushin E and Görling A 2017 Understanding band gaps of solids in generalized Kohn–Sham theory *Proceedings of the National Academy of Sciences* 114 2801
- [24] Pettes Michael T and Shi L 2009 Thermal and Structural Characterizations of Individual Single□, Double□, and Multi□Walled Carbon Nanotubes Advanced Functional Materials 19 3918-25
- [25] Reed M L, El-Masry N A, Stadelmaier H H, Ritums M K, Reed M J, Parker C A, Roberts J C and Bedair S M 2001 Room temperature ferromagnetic properties of (Ga, Mn)N *Applied Physics Letters* **79** 3473-5
- [26] Seo K, Bagkar N, Kim S-i, In J, Yoon H, Jo Y and Kim B 2010 Diffusion-Driven Crystal Structure Transformation: Synthesis of Heusler Alloy Fe3Si Nanowires *Nano Letters* **10** 3643-7
- [27] Seo K, Varadwaj K S K, Mohanty P, Lee S, Jo Y, Jung M-H, Kim J and Kim B 2007 Magnetic

- Properties of Single-Crystalline CoSi Nanowires *Nano Letters* **7** 1240-5
- [28] Seo K, Yoon H, Ryu S-W, Lee S, Jo Y, Jung M-H, Kim J, Choi Y-K and Kim B 2010 Itinerant Helimagnetic Single-Crystalline MnSi Nanowires *ACS Nano* 4 2569-76
- [29] Sham L and Schlüter M 1983 Density-functional theory of the energy gap *Physical Review Letters* **51** 1888
- [30] Sharma P, Gupta A, Rao K V, Owens F J, Sharma R, Ahuja R, Guillen J M O, Johansson B and Gehring G A 2003 Ferromagnetism above room temperature in bulk and transparent thin films of Mn-doped ZnO *Nature Materials* **2** 673
- [31] Sievers S, Braun K F, Eberbeck D, Gustafsson S, Olsson E, Schumacher Hans W and Siegner U 2012 Quantitative Measurement of the Magnetic Moment of Individual Magnetic Nanoparticles by Magnetic Force Microscopy *Small* **8** 2675-9
- [32] Sun L, Hao Y, Chien C L and Searson P C 2005 Tuning the properties of magnetic nanowires *IBM Journal of Research and Development* **49** 79-102
- [33] Thelander C, Agarwal P, Brongersma S, Eymery J, Feiner L F, Forchel A, Scheffler M, Riess W, Ohlsson B J, Gösele U and Samuelson L 2006 Nanowire-based one-dimensional electronics *Materials Today* 9 28-35
- [34] Tomczak J M, Haule K and Kotliar G 2012 Signatures of electronic correlations in iron silicide Proceedings of the National Academy of Sciences 109 3243
- [35] van Arkel A E and de Boer J H 1925 Darstellung von reinem Titanium-, Zirkonium-, Hafnium- und Thoriummetall Zeitschrift für anorganische und allgemeine Chemie 148 345-50
- [36] Wolfe R, Wernick J H and Haszko S E 1965 Thermoelectric properties of FeSi *Physics Letters* 19 449-50
- [37] Z W Lu and B M Klein and Zhu-Pei Shi V R G a E Z K a V M C a Y M Y a S N S a A V P a S U a M N a 1995 Electronic structure of FeSi Journal of Physics: Condensed Matter 7 5529
- [38] Zhao L-D, Lo S-H, Zhang Y, Sun H, Tan G, Uher C, Wolverton C, Dravid V P and Kanatzidis M G 2014 Ultralow thermal conductivity and high thermoelectric figure of merit in SnSe crystals *Nature* **508** 373-7